Measurement Science and
Technology

PAPER • **OPEN ACCESS**

Polar transfer alignment of shipborne SINS with a large misalignment angle

To cite this article: Jianhua Cheng *et al* 2016 *Meas. Sci. Technol.* **27** 035101

View the article online for updates and enhancements.

You may also like

- Unscented Kalman filter (UKF)–based nonlinear parameter estimation for a turbulent boundary layer: a data assimilation framework
Zhao Pan, Yang Zhang, Jonas P R Gustavsson et al.
- UKF-based MEMS micromirror angle estimation for LiDAR
Junya Wang, Gaofei Zhang and Zheng You
- Tracking the effects of propofol, sevoflurane and (S)-ketamine anesthesia using an unscented Kalman filter-based neural mass model
Zhenhu Liang, Dihuan Wang, Xing Jin et al.

This content was downloaded from IP address 202.8.112.197 on 06/07/2023 at 07:13

OPEN ACCESS
IOP Publishing
Measurement Science and Technology
Meas. Sci. Technol. **27** (2016) 035101 (12pp)
doi:10.1088/0957-0233/27/3/035101

Polar transfer alignment of shipborne SINS with a large misalignment angle

Jianhua Cheng, Tongda Wang, Dongxue Guan and Meiling Li

Marine Navigation Research Institute, College of Automation, Harbin Engineering University, Harbin 150001, People's Republic of China

E-mail: ins_wtd@163.com

Received 17 November 2015, revised 14 December 2015
Accepted for publication 21 December 2015
Published 14 January 2016

Abstract

Existing polar transfer alignment (TA) algorithms are designed based on linear Kalman filters (KF) to estimate misalignment angles. In the case of a large misalignment angle, these algorithms cannot be applied in order to achieve accurate TA. In this paper, a TA algorithm based on an unscented Kalman filter (UKF) is proposed to solve the problem of the large misalignment angle in the polar region. Based on a large misalignment angle, nonlinear navigation error equations, which are the UKF dynamic models, are derived under grid frames. This paper chooses the velocity plus attitude matching method as the TA matching method and errors of velocity and attitude as observations. The misalignment angle can be estimated by the designed UKF. The simulation results have demonstrated that the polar TA algorithm can be effective in improving the TA accuracy, especially when large misalignment angles occur.

Keywords: transfer alignment, large misalignment angle, grid frame, UKF

(Some figures may appear in colour only in the online journal)

1. Introduction

Polar navigation technology can ensure the safety and reliability of a ship when it sails in a polar region [1]. Traditional electromagnetic navigation suffers from serious magnetic disturbances in polar regions [2]. Similarly, in a high latitude area, the multipath effect [3] may decrease the positioning accuracy of a global positioning system (GPS) and even cause a failure of the GPS. However, a inertial navigation system (INS) is highly autonomous and self-contained [4], and it can address the serious challengesposed by polar environments [5]. Therefore, INS is the optimal choice for civil and military navigation in polar regions.

As a key technology of the Strapdown INS (SDINS), the initial alignment is to obtain an initial attitude matrix before navigation [6]. The performance of initial alignment directly affects the following navigation accuracy [7]. Currently, transfer alignment (TA) is an initial alignment method which has been widely researched. The basic idea of TA is using a high-precision master SDINS output to match low-precision salve SDINS motion parameters, and then estimate the states of alignment by using a filter algorithm. TA based on the velocity plus attitude matching method [8] has the advantages of both rapid speed and low cost, and it has been used in shipboard aircrafts and for shipborne weapons alignment [9].

When TA operates in the polar regions, three problems should be addressed. First, meridian lines converge in the pole in the polar region, which motivates the selection problem of the navigation frame. A traditional north-oriented frame loses its effectiveness for polar navigation, since in this frame navigation error increase sharply due to the meridian convergence [10]. As a primary solution, the wander frame was selected for the polar navigation problem. However, the definition of the wander angle is ineffective at a 90-degree latitude [1, 10]. Therefore, it is necessary to choose a suitable frame for the polar region. Secondly, TA can be classified as coarse and fine alignment according to the alignment stages. A Kalman filter (KF) is commonly employed in fine alignment to estimate misalignment angles. The existing KF models are linear based on

Original content from this work may be used under the terms of the Creative Commons Attribution 3.0 licence. Any further distribution of this work must maintain attribution to the author(s) and the title of the work, journal citation and DOI.

 © 2016 IOP Publishing Ltd Printed in the UK

the small-misalignment-angle assumption. This assumption will be invalid if the azimuth misalignment angle is large due to ship deformation and inaccurate coarse alignment. Hence, the filter models change to be nonlinear and need to be redesigned. Thirdly, corresponding to the nonlinear models, a suitable nonlinear filtering algorithm should replace the linear KF.

To select a suitable frame for polar navigation, a transverse frame is proposed in [10]. This frame solves the position and azimuth determining problem by moving the earth's pole artificially to the equator. However, the frame is derived based on the assumption that the earth is round, so it can lead to principle calculation errors. In [11], a navigation algorithm is designed based on grid frame for flight navigation in polar regions. In the grid frame, an available reference line is set for determining the azimuth angle. Grid navigation can solve the problem of the meridians convergence. Therefore, a grid frame is suitable for developing navigation algorithms when SDINS works in polar regions.

A TA algorithm using grid frame is presented in [12]. The TA algorithm based on a grid frame can be applied to the aerial alignment of airborne weapons in polar alignment, and it can perform with high accuracy. However, the linear models in TA are designed based on the hypothesis of small attitude errors. When the azimuth misalignment angle is large, the KF models will be inaccurate and cause the remarkable errors of TA alignment. To estimate attitude errors, nonlinear KF models are introduced based on a large azimuth misalignment angle [13, 14]. The existing TA algorithm [14] adopts a north-oriented frame as a navigation frame to construct the nonlinear models, but it cannot be used for polar TA. Therefore, nonlinear models need to be redesigned based on grid frames for the polar TA.

A nonlinear estimator is required to process the nonlinear models. An extended Kalman filter (EKF) is used for nonlinear models in [15] to realize the TA of an airborne vehicle. However, the linearization error of the nonlinear model in EKF will reduce the precision of the filter, and even cause the filter divergence when the model is strongly nonlinear. A rapid TA algorithm based on an unscented Kalman filter (UKF) is proposed in [16], and the UKF can provide more accurate estimates than the EKF. Therefore, the UKF is chosen as estimation method of TA in this paper.

In this paper, a polar TA algorithm based on UKF is proposed. The main purpose of this paper is to solve the problem of a large azimuth misalignment angle in the polar TA. Combined with the velocity plus attitude matching method, grid-frame-based nonlinear models are derived. Then, a UKF is employed to estimate alignment states, which can improve the accuracy of the polar TA.

2. Grid navigation error equations with a large azimuth misalignment angle

In the grid frame, the Greenwich meridian is the reference for determining the azimuth angle. Choosing the grid frame as the navigation frame can avoid the problems caused by the meridian convergence in high latitude areas.

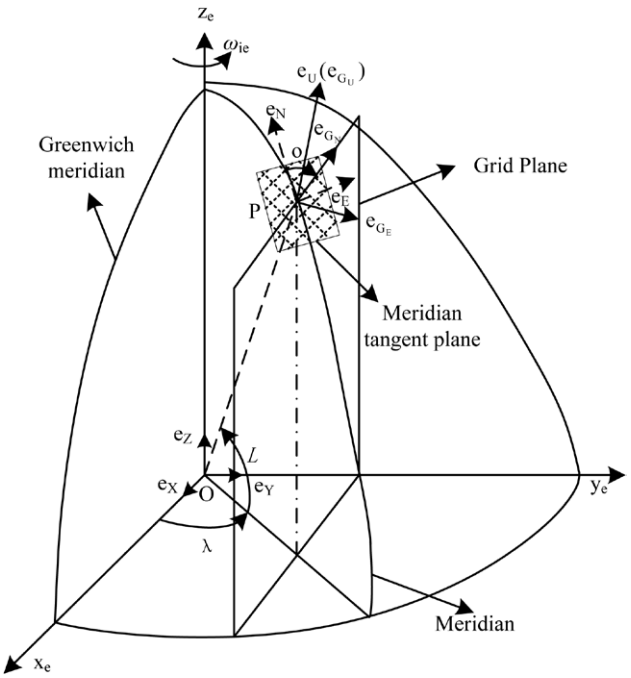

Figure 1. The description of the grid frame.

2.1. Grid frames

The notations of frames used in this paper are:

i-inertial frame;
e-earth centered earth fixed frame;
t-geographic frame;
G-grid frame;
m-body frame of master SDINS;
s-body frame of slave SDINS;
s′-calculated body frame of slave SDINS.

The Grid frame is the navigation frame. The *s* frame represents the true body frame of slave SDINS. Considering the measurements biases, the *s′* frame is the calculated body frame of slave SDINS.

As shown in figure 1, when a ship is located on point *P*, the grid plane is the plane which passes through point *P* and is parallel with the Greenwich plane. The grid north axis lies along the intersecting line of the grid plane and local-level. The angle between true north and the grid north axis is σ. The grid up axis coincides with the geographic up axis. The grid east axis lies in level and is perpendicular to the grid north axis. Grid east and grid north axis constitute the right frame that is called grid frame. The set of unit vectors along grid east, north and up axis are presented as $(\mathbf{e}_{G_E}, \mathbf{e}_{G_N}, \mathbf{e}_{G_U})$.

The latitude and longitude of point *P* are defined as *L* and λ, respectively. The transformation relations among *e* frame, *t* frame and *G* frame can be described as:

$$\boldsymbol{C}_e^t = \begin{bmatrix} -\sin\lambda & \cos\lambda & 0 \\ -\sin L\cos\lambda & -\sin L\sin\lambda & \cos L \\ \cos L\cos\lambda & \cos L\sin\lambda & \sin L \end{bmatrix} \tag{1}$$

$$\boldsymbol{C}_t^G = \begin{bmatrix} \cos\sigma & -\sin\sigma & 0 \\ \sin\sigma & \cos\sigma & 0 \\ 0 & 0 & 1 \end{bmatrix} \tag{2}$$

The set of unit vectors along each axis of the t and e frame are presented as $(\mathbf{e}_E, \mathbf{e}_N, \mathbf{e}_U)$ and $(\mathbf{e}_X, \mathbf{e}_Y, \mathbf{e}_Z)$, respectively. According to figure 1, $\mathbf{e}_{G_N}$ is perpendicular to $\mathbf{e}_Y$, and thus the inner product of them equals zero:

$$\mathbf{e}_{G_N} \cdot \mathbf{e}_Y = 0 \tag{3}$$

By transforming $\mathbf{e}_{G_N}$ and $\mathbf{e}_Y$ to the t frame, $\mathbf{e}^t_{G_N}$and $\mathbf{e}^t_Y$ can be expressed as:

$$\mathbf{e}^t_{G_N} = \boldsymbol{C}^t_G \mathbf{e}^G_{G_N} = [\sin\sigma \quad \cos\sigma \quad 0]^T \tag{4}$$

$$\mathbf{e}^t_Y = \boldsymbol{C}^t_e \mathbf{e}^e_Y = [\cos\lambda \quad -\sin L \sin\lambda \quad \cos L \sin\lambda]^T \tag{5}$$

By substituting equations (4) and (5) into (3), we can obtain:

$$\sin\sigma\cos\lambda - \cos\sigma \sin L \sin\lambda = 0 \tag{6}$$

Then,

$$\sin\sigma = \sin\lambda \sin L / \sqrt{1 - \cos^2 L \sin^2\lambda} \tag{7}$$

$$\cos\sigma = \cos\lambda / \sqrt{1 - \cos^2 L \sin^2\lambda} \tag{8}$$

By substituting equations (7) and (8) into (2) the transformation matrix $\boldsymbol{C}^G_t$ from t to G frame can be calculated.

The INS error equations in [11, 12] are derived based on the grid frame. During both the derivation of error equations, misalignment angles are considered as small angles. However, small angle assumption is inconsistent as the result of flexure deformation and coarse alignment in practice. In the case of large azimuth misalignment angle, the INS error equations are modified in the subsections.

2.2. Attitude error equation

Flexure deformation and inaccurate coarse alignment may cause large misalignment angles, especially large azimuth misalignment angles. The initial attitude matrix of the slave SDINS is unknown when it starts to work. The coarse initial attitude matrix of the slave SDINS is commonly provided by the initial attitude matrix of the master SDINS:

$$\boldsymbol{C}^G_m(0) = \boldsymbol{C}^G_s(0) \tag{9}$$

Where $\boldsymbol{C}^G_s$ represents the calculated attitude matrix of the slave SDINS from s' to G frame.

The master and slave SDINS are not installed on the same base, so there are misalignment angles among the different bases. We define the angles between the s' frame and the m frame as measurement misalignment angles $\boldsymbol{\phi}^G_m = \begin{bmatrix} \phi^G_{mx} & \phi^G_{my} & \phi^G_{mz} \end{bmatrix}^T$. We define angles between the s frame and m frame as actual physical misalignment angles $\boldsymbol{\phi}^G_a = \begin{bmatrix} \phi^G_{ax} & \phi^G_{ay} & \phi^G_{az} \end{bmatrix}^T$. The pitch and roll misalignment angles of $\boldsymbol{\phi}^G_m$ (i.e. ϕ^G_{mx} and ϕ^G_{my}) and $\boldsymbol{\phi}^G_a$ (i.e. ϕ^G_{ax} and ϕ^G_{ay}) can be considered as small angles, but the azimuth misalignment angles ϕ^G_{mz} and ϕ^G_{az} are large.

The s' frame can be obtained by the following three-time rotation of the m frame:

$$\begin{aligned} Ox_m y_m z_m &\xrightarrow[\phi^G_{mz}]{\text{around } z_m \text{ axis}} Ox'_m y'_m z'_m \\ &\xrightarrow[\phi^G_{mx}]{\text{around } x'_m \text{ axis}} Ox''_m y''_m z''_m \\ &\xrightarrow[\phi^G_{my}]{\text{around } y''_m \text{ axis}} Ox_{s'} y_{s'} z_{s'} \end{aligned} \tag{10}$$

The first rotation performs around the z_m axis by ϕ^G_{mz}, which generates the frame $Ox'_m y'_m z'_m$. The second one is the rotation of the x'_m axis by ϕ^G_{mx}, which generates the frame $Ox''_m y''_m z''_m$. The third rotation acts around the y''_m axis by ϕ^G_{my}, which generates the frame $Ox_{s'} y_{s'} z_{s'}$.

The direction cosine matrix between the s' and m frame can be expressed as:

$$\boldsymbol{C}^{s'}_m = \boldsymbol{C}_{\phi^G_{my}} \boldsymbol{C}_{\phi^G_{mx}} \boldsymbol{C}_{\phi^G_{mz}} = \begin{bmatrix} c\phi^G_{my} c\phi^G_{mz} - s\phi^G_{mx} s\phi^G_{my} c\phi^G_{mz} & c\phi^G_{my} s\phi^G_{mz} + s\phi^G_{mx} s\phi^G_{my} c\phi^G_{mz} & -c\phi^G_{mx} s\phi^G_{my} \\ -c\phi^G_{mx} s\phi^G_{mz} & c\phi^G_{mx} c\phi^G_{mz} & s\phi^G_{mx} \\ s\phi^G_{my} c\phi^G_{mz} + s\phi^G_{mx} c\phi^G_{my} s\phi^G_{mz} & s\phi^G_{my} s\phi^G_{mz} - s\phi^G_{mx} c\phi^G_{my} c\phi^G_{mz} & c\phi^G_{mx} c\phi^G_{my} \end{bmatrix} \tag{11}$$

Where the notation c and s represent cosine and sine functions, respectively. Similarly, the direction cosine matrix between s and m frame can be described as:

$$\boldsymbol{C}^s_m = \boldsymbol{C}_{\phi^G_{ay}} \boldsymbol{C}_{\phi^G_{ax}} \boldsymbol{C}_{\phi^G_{az}} = \begin{bmatrix} c\phi^G_{ay} c\phi^G_{az} - s\phi^G_{ax} s\phi^G_{ay} c\phi^G_{az} & c\phi^G_{ay} s\phi^G_{az} + s\phi^G_{ax} s\phi^G_{ay} c\phi^G_{az} & -c\phi^G_{ax} s\phi^G_{ay} \\ -c\phi^G_{ax} s\phi^G_{az} & c\phi^G_{ax} c\phi^G_{az} & s\phi^G_{ax} \\ s\phi^G_{ay} c\phi^G_{az} + s\phi^G_{ax} c\phi^G_{ay} s\phi^G_{az} & s\phi^G_{ay} s\phi^G_{az} - s\phi^G_{ax} c\phi^G_{ay} c\phi^G_{az} & c\phi^G_{ax} c\phi^G_{ay} \end{bmatrix} \tag{12}$$

The angular velocity of m frame relative to s' frame is $\boldsymbol{\omega}_{ms'}$, and the projection of $\boldsymbol{\omega}_{ms'}$ on s' frame can be expressed as follows:

$$\begin{aligned} \boldsymbol{\omega}^{s'}_{ms'} = &\begin{bmatrix} c\phi^G_{my} & 0 & -s\phi^G_{my} \\ 0 & 1 & 0 \\ s\phi^G_{my} & 0 & c\phi^G_{my} \end{bmatrix} \begin{bmatrix} 1 & 0 & 0 \\ 0 & c\phi^G_{mx} & s\phi^G_{mx} \\ 0 & -s\phi^G_{mx} & c\phi^G_{mx} \end{bmatrix} \begin{bmatrix} 0 \\ 0 \\ \dot{\phi}^G_z \end{bmatrix} \\ &+ \begin{bmatrix} c\phi^G_{my} & 0 & -s\phi^G_{my} \\ 0 & 1 & 0 \\ s\phi^G_{my} & 0 & c\phi^G_{my} \end{bmatrix} \begin{bmatrix} \dot{\phi}^G_{mx} \\ 0 \\ 0 \end{bmatrix} + \begin{bmatrix} \dot{\phi}^G_{my} \\ 0 \\ 0 \end{bmatrix} \end{aligned} \tag{13}$$

By using the matrix inversion lemma, $\boldsymbol{\phi}^G_m$ can be concluded by:

$$\dot{\boldsymbol{\phi}}_m^G = f(\boldsymbol{\phi}_m^G)\boldsymbol{\omega}_{ms'}^{s'} \tag{14}$$

Where

$$f((\boldsymbol{\phi})_m^G) = \begin{bmatrix} c\phi_{my}^G & 0 & -c\phi_{mx}^G s\phi_{my}^G \\ 0 & 1 & s\phi_{mx}^G \\ s\phi_{my}^G & 0 & c\phi_{mx}^G c\phi_{my}^G \end{bmatrix} \tag{15}$$

Also, $\boldsymbol{\omega}_{ms'}^{s'}$ equals to:

$$\boldsymbol{\omega}_{ms'}^{s'} = \boldsymbol{\omega}_{Gs'}^{s'} - \boldsymbol{\omega}_{Gm}^{s'} = \boldsymbol{\omega}_{Gs'}^{s'} - \boldsymbol{C}_m^{s'}\boldsymbol{\omega}_{Gm}^m \tag{16}$$

The true angular velocity of s frame relative to G frame is $\boldsymbol{\omega}_{Gs}$, and the projection of $\boldsymbol{\omega}_{Gs}$ on s frame can be written as:

$$\boldsymbol{\omega}_{Gs}^s = \boldsymbol{\omega}_{Gm}^s + \boldsymbol{\omega}_f \tag{17}$$

Where $\boldsymbol{\omega}_{Gm}$ is the angular velocity of the G frame relative to the m frame, and $\boldsymbol{\omega}_{Gm}^s$ is the projection of $\boldsymbol{\omega}_{Gm}$ on the s frame; $\boldsymbol{\omega}_f$ is the flexure deformation angular velocity of slave SDINS caused by elastic deformation.

Considering the gyro drifts $\delta\boldsymbol{\omega}_{is}^s$, the measured angular velocity of the G frame relative to the s' frame can be written as

$$\boldsymbol{\omega}_{Gs'}^{s'} = \boldsymbol{\omega}_{Gs}^s - \delta\boldsymbol{\omega}_{is}^s \tag{18}$$

By substituting equations (17) into (18), we can obtain:

$$\boldsymbol{\omega}_{Gs'}^{s'} = \boldsymbol{\omega}_{Gm}^s + \boldsymbol{\omega}_f - \delta\boldsymbol{\omega}_{is}^s \tag{19}$$

The gyro drifts of the slave SDINS $\delta\boldsymbol{\omega}_{is}^s$ can be modeled as:

$$\delta\boldsymbol{\omega}_{is}^s = \boldsymbol{\varepsilon}_s^s + \boldsymbol{\varepsilon}_w^s \tag{20}$$

Where $\boldsymbol{\varepsilon}_s^s$ is the gyro constant drift, and $\boldsymbol{\varepsilon}_w^s$ is the gyro random drift.

By combining the equations (16)–(18), $\boldsymbol{\omega}_{ms'}^{s'}$ can be rewritten as:

$$\begin{aligned} \boldsymbol{\omega}_{ms'}^{s'} &= \boldsymbol{\omega}_{Gm}^s + \boldsymbol{\omega}_f - \boldsymbol{C}_{s'}^G\delta\boldsymbol{\omega}_{is}^s - \boldsymbol{C}_m^{s'}\boldsymbol{\omega}_{Gm}^m \\ &= (\boldsymbol{C}_m^s - \boldsymbol{C}_m^{s'})\boldsymbol{\omega}_{Gm}^m + \boldsymbol{\omega}_f - \boldsymbol{\varepsilon}_s^s - \boldsymbol{\varepsilon}_w^s \end{aligned} \tag{21}$$

Based on the small ϕ_{mx}^G, ϕ_{my}^G, ϕ_{ax}^G and ϕ_{ay}^G angles, $f(\boldsymbol{\phi}_m^G)$ can be simplified as a $\boldsymbol{I}_{3\times3}$. Meanwhile, $\boldsymbol{C}_m^{s'}$ and $\boldsymbol{C}_m^s$ in equations (11) and (12) can be simplified as:

$$\boldsymbol{C}_m^{s'} = \begin{bmatrix} c\phi_{mz}^G & s\phi_{mz}^G & -\phi_{my}^G \\ -s\phi_{mz}^G & c\phi_{mz}^G & \phi_{mx}^G \\ \phi_{my}^G c\phi_{mz}^G + \phi_{mx}^G s\phi_{mz}^G & \phi_{my}^G s\phi_{mz}^G - \phi_{mx}^G c\phi_{mz}^G & 1 \end{bmatrix} \tag{22}$$

$$\boldsymbol{C}_m^s = \begin{bmatrix} c\phi_{az}^G & s\phi_{az}^G & -\phi_{ay}^G \\ -s\phi_{az}^G & c\phi_{az}^G & \phi_{ax}^G \\ \phi_{ay}^G c\phi_{az}^G + \phi_{ax}^G s\phi_{az}^G & \phi_{ay}^G s\phi_{az}^G - \phi_{ax}^G c\phi_{az}^G & 1 \end{bmatrix} \tag{23}$$

By substituting $f(\boldsymbol{\phi}_m^G) = \boldsymbol{I}_{3\times3}$ into equation (14), it can be obtained that $\dot{\boldsymbol{\phi}}_m^G = \boldsymbol{\omega}_{ms'}^{s'}$. Then, in the case of the large azimuth misalignment angle, the attitude error equation can be expressed by using equations (19)–(21) as:

$$\dot{\boldsymbol{\phi}}_m^G = (\boldsymbol{C}_m^{s'} - \boldsymbol{C}_m^s)\boldsymbol{\omega}_{Gm}^m + \boldsymbol{\omega}_f - \boldsymbol{\varepsilon}_s^s - \boldsymbol{\varepsilon}_w^s \tag{24}$$

The relative position between the master and slave SDINS is fixed. Therefore, the actual physical misalignment angle $\boldsymbol{\phi}_a^G$ can be considered as a constant. Then, its differential equation is:

$$\dot{\boldsymbol{\phi}}_a^G = 0 \tag{25}$$

2.3. Velocity error equation

The velocity differential equations of master and slave SDINS based on G frame can be written as:

$$\dot{\boldsymbol{V}}_m^G = \boldsymbol{C}_m^G\boldsymbol{f}^m - (2\boldsymbol{\omega}_{ie}^G + \boldsymbol{\omega}_{eG}^G) \times \boldsymbol{V}_m^G + \boldsymbol{g}_m^G \tag{26}$$

$$\dot{\boldsymbol{V}}_s^G = \boldsymbol{C}_s^G\boldsymbol{f}^s - (2\boldsymbol{\omega}_{ie}^G + \boldsymbol{\omega}_{eG}^G) \times \boldsymbol{V}_s^G + \boldsymbol{g}_s^G \tag{27}$$

Where $\dot{\boldsymbol{V}}_m^G$ and $\dot{\boldsymbol{V}}_s^G$ are velocities of master and slave SDINS, $\boldsymbol{f}^m$ and $\boldsymbol{f}^s$ are specific force measured by master and slave SDINS accelerometers, $\boldsymbol{\omega}_{ie}^G$ is the projection of rotational angular velocity of the earth on G frame, $\boldsymbol{\omega}_{eG}$ is angular velocity of e frame relative to G frame, $\boldsymbol{\omega}_{eG}^G$ is the projection of $\boldsymbol{\omega}_{eG}$ on G frame, $\boldsymbol{g}_m$ and $\boldsymbol{g}_s$ are the gravity measured by master and slave SDINS, $\boldsymbol{g}_m^G$ and $\boldsymbol{g}_s^G$ are the projections of $\boldsymbol{g}_m$ and $\boldsymbol{g}_s$ on G frame, respectively. $\boldsymbol{\omega}_{ie}^G$ can be obtained by:

$$\boldsymbol{\omega}_{ie}^G = \boldsymbol{C}_g^G\boldsymbol{\omega}_{ie}^g \tag{28}$$

As shown in [12], $\boldsymbol{\omega}_{eG}^G$ can be expressed as:

$$\boldsymbol{\omega}_{eG}^G = \begin{bmatrix} \omega_{eGx}^G \\ \omega_{eGy}^G \\ \omega_{eGz}^G \end{bmatrix} = \begin{bmatrix} \dfrac{v_{G_\mathrm{E}}}{\tau_f} - \dfrac{v_{G_\mathrm{N}}}{R_y} \\ \dfrac{v_{G_\mathrm{E}}}{R_x} - \dfrac{v_{G_\mathrm{N}}}{\tau_f} \\ \dfrac{\kappa v_{G_\mathrm{E}}}{\tau_f} - \dfrac{\kappa v_{G_\mathrm{N}}}{R_y} \end{bmatrix} \tag{29}$$

Where v_{G_E} and v_{G_N} are the east and north velocity of the ship within G frame. Other parameters are defined as follows:

$$\begin{cases} \dfrac{1}{R_x} = \dfrac{\sin^2\sigma}{R_{Mh}} + \dfrac{\cos^2\sigma}{R_{Nh}}, \\ \dfrac{1}{R_y} = \dfrac{\cos^2\sigma}{R_{Mh}} + \dfrac{\sin^2\sigma}{R_{Nh}}, \\ \dfrac{1}{\tau_f} = \left(\dfrac{1}{R_{Mh}} - \dfrac{1}{R_{Nh}}\right)\sin\sigma\cos\sigma, \\ \kappa = \dfrac{\sin\lambda\cos L}{\sqrt{1-\cos^2 L\sin^2\lambda}}. \end{cases} \tag{30}$$

Where R_{Mh} and R_{Nh} are radius of curvature in meridian and prime vertical, respectively.

Because G frame also has a local horizontal plane, $\boldsymbol{g}^G$ can be expressed as:

$$\boldsymbol{g}^G = \begin{bmatrix} 0 & 0 & -g \end{bmatrix}^T \tag{31}$$

Considering measurement errors, the velocity differential equation of the slave SDINS can be rewritten as:

$$\dot{\boldsymbol{V}}_{s'}^G = \boldsymbol{C}_s^G \boldsymbol{f}^s - (2\widehat{\boldsymbol{\omega}}_{ie}^G + \widehat{\boldsymbol{\omega}}_{eG}^G) \times \boldsymbol{V}_{s'}^G + \widehat{\boldsymbol{g}}_{s'}^G \tag{32}$$

Where $\boldsymbol{V}_{s'}^G$, $\widehat{\boldsymbol{\omega}}_{ie}^G$, $\widehat{\boldsymbol{\omega}}_{eG}^G$ and $\widehat{\boldsymbol{g}}_{s'}^G$ are measured by slave SDINS, and the measurement errors of $\boldsymbol{\omega}_{ie}^G$, $\boldsymbol{\omega}_{eG}^G$ and $\boldsymbol{g}_{s'}^G$ are described as $\delta\boldsymbol{\omega}_{ie}^G = \widehat{\boldsymbol{\omega}}_{ie}^G - \boldsymbol{\omega}_{ie}^G$, $\delta\boldsymbol{\omega}_{eG}^G = \widehat{\boldsymbol{\omega}}_{eG}^G - \boldsymbol{\omega}_{eG}^G$, and $\delta\boldsymbol{g}_{s'}^G = \widehat{\boldsymbol{g}}_{s'}^G - \boldsymbol{g}_{s'}^G$, respectively.

The velocity error in TA is defined as $\delta\boldsymbol{V}^G = \boldsymbol{V}_{s'}^G - \boldsymbol{V}_m^G$. By subtracting equations (26) from (32) and neglecting the small second-order amount, the velocity error equation can be presented as:

$$\begin{aligned}\delta\dot{\boldsymbol{V}}^G = {} & \boldsymbol{C}_s^G \boldsymbol{f}^s - \boldsymbol{C}_m^G \boldsymbol{f}^m - (2\boldsymbol{\omega}_{ie}^G + \boldsymbol{\omega}_{eG}^G) \times \delta\boldsymbol{V}^G \\ & -(2\delta\boldsymbol{\omega}_{ie}^G + \delta\boldsymbol{\omega}_{eG}^G) \times \boldsymbol{V}_{s'}^G + \boldsymbol{g}_{s'}^G - \boldsymbol{g}_m^G + \delta\boldsymbol{g}_{s'}^G\end{aligned} \tag{33}$$

In the practice environment, the gravity measured by the master and slave SDINS can be considered equal, so it can be concluded that:

$$\boldsymbol{g}_{s'}^G = \boldsymbol{g}_m^G \tag{34}$$

The specific force measured by the slave SDINS accelerometers can be written as:

$$\boldsymbol{f}^s = \boldsymbol{C}_m^s \boldsymbol{f}^m + \delta\boldsymbol{f}^s + \nabla_s^s \tag{35}$$

Where $\delta\boldsymbol{f}^s$ is the disturbing acceleration caused by arm-lever effect and ship flexure deformation, and ∇_s^s represents the constant bias of the accelerometer. Then, the velocity error equation can be rewritten as:

$$\begin{aligned}\delta\dot{\boldsymbol{V}}^G = {} & (\boldsymbol{C}_{s'}^G - \boldsymbol{C}_s^G)\boldsymbol{f}^s - (2\boldsymbol{\omega}_{ie}^G + \boldsymbol{\omega}_{eG}^G) \times \delta\boldsymbol{V}^G \\ & -(2\delta\boldsymbol{\omega}_{ie}^G + \delta\boldsymbol{\omega}_{eG}^G) \times \boldsymbol{V}_{s'}^G + \boldsymbol{C}_s^G \delta\boldsymbol{f} + \boldsymbol{C}_{s'}^G \nabla_s^s + \delta\boldsymbol{g}_{s'}^G\end{aligned} \tag{36}$$

3. The design of nonlinear models for polar TA

In TA, the high-precision master SDINS outputs are transferred to assist the alignment of the low-precision salve SDINS. The misalignment parameters of the slave SDINS relative to the master SDINS are estimated by the KF.

For nonlinear models, the UKF is used to accomplish the TA. This way, the polar TA can be precisely achieved. Also the system robustness can be improved by solving the problem of the large azimuth misalignment angle in practical environments.

In TA, the outputs of the master SDINS are assumed to be accurate and without error. The dynamic model is designed based on the error equations of grid navigation, and the observation model is designed based on the velocity and attitude measurements. The detailed design of the filter models are presented in the following subsections.

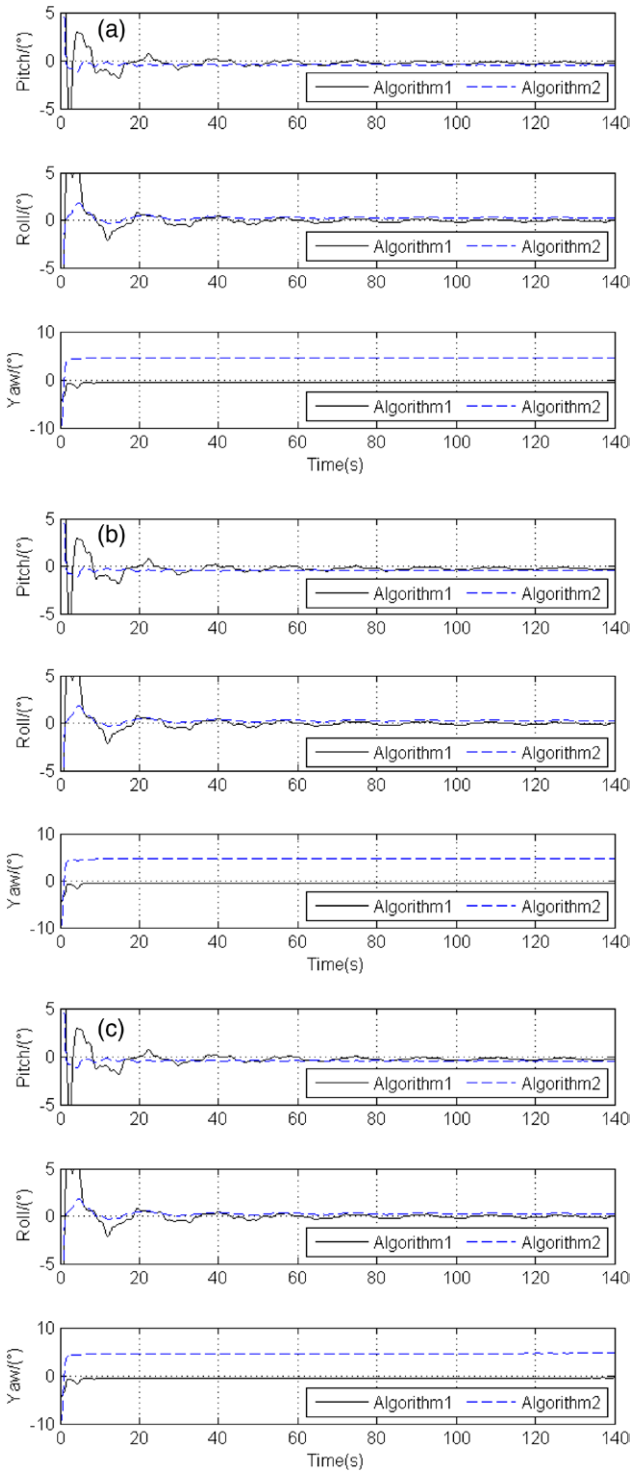

Figure 2. (a) TA results when ship is static. (b) TA results when ship sails in uniform linear motion. (c) TA results when ship sails is in linear motion with constant acceleration.

3.1. Dynamic model

Based on the G frame, the errors of velocity $\delta\boldsymbol{V}^G$, the measurement misalignment angles $\boldsymbol{\phi}_m^G$, the constant biases of gyros $\boldsymbol{\varepsilon}_s^s$

Table 1. TA results in the calm sea state.

Parameters	Algorithm	Static	Uniform linear motion	Linear motion with constant acceleration
pitch/(°)	Algorithm 1	−0.2811	−0.2811	−0.2846
	Algorithm 2	−0.4589	−0.4597	−0.4637
roll/(°)	Algorithm 1	−0.0295	−0.0303	−0.0266
	Algorithm 2	0.2508	0.2498	0.2548
yaw/(°)	Algorithm 1	−0.5225	−0.5225	0.4405
	Algorithm 2	4.579	4.579	4.683

Table 2. TA results in the medium sea state.

Parameters	Algorithm	Static	Uniform linear motion	Linear motion with constant acceleration
pitch /(°)	Algorithm 1	−0.0646	−0.0644	−0.0570
	Algorithm 2	−0.3707	−0.3720	−0.3728
roll/(°)	Algorithm 1	−0.0113	−0.0121	−0.0119
	Algorithm 2	0.2114	0.2281	0.2271
yaw/(°)	Algorithm 1	−0.4809	−0.4809	−0.3972
	Algorithm 2	3.872	3.972	3.972

and accelerometers ∇_s^s, and the actual physical misalignment angles $\boldsymbol{\phi}_a^G$ are chosen as the states to be estimated, which are described as:

$$\boldsymbol{X} = \begin{bmatrix} \delta \boldsymbol{V}^G & \boldsymbol{\phi}_m^G & \boldsymbol{\varepsilon}_s^s & \boldsymbol{\nabla}_s^s & \boldsymbol{\phi}_a^G \end{bmatrix}^T$$

According to the derived error equations of attitude (i.e. equations (22) and (23)) and velocity (i.e. equation (34)), neglecting the measurement errors of gravity, the differential equations of the states can be written as:

$$\begin{cases} \delta \dot{\boldsymbol{V}}^G = (\boldsymbol{C}_{s'}^G - \boldsymbol{C}_s^G)\boldsymbol{f}^s - (2\boldsymbol{\omega}_{ie}^G + \boldsymbol{\omega}_{eG}^G) \times \delta \boldsymbol{V}_{s'}^G \\ \qquad\qquad -(2\delta\boldsymbol{\omega}_{ie}^G + \delta\boldsymbol{\omega}_{eG}^G) \times \boldsymbol{V}^G + \boldsymbol{C}_{s'}^G \delta \boldsymbol{f} + \boldsymbol{C}_{s'}^G \nabla_s^s \\ \dot{\boldsymbol{\phi}}_m^G = (\boldsymbol{C}_m^s - \boldsymbol{C}_m^{s'})\boldsymbol{\omega}_{Gm}^m + \boldsymbol{\omega}_f - \boldsymbol{\varepsilon}_s^s - \boldsymbol{\varepsilon}_w^s \\ \dot{\boldsymbol{\nabla}}_s^s = 0 \\ \dot{\boldsymbol{\varepsilon}}_s^s = 0 \\ \dot{\boldsymbol{\phi}}_a^G = 0 \end{cases} \tag{37}$$

The above dynamic model for the polar TA is defined as Model 1. Meanwhile, the typical dynamic model for non-polar TA, which is presented in [14], is defined as Model 2. Model 2 is also designed by considering the large azimuth alignment angle, which is expressed as:

$$\begin{cases} \delta \dot{\boldsymbol{V}}^t = (\boldsymbol{C}_{s'}^t - \boldsymbol{C}_s^t)\boldsymbol{f}^s - (2\boldsymbol{\omega}_{ie}^t + \boldsymbol{\omega}_{et}^t) \times \delta \boldsymbol{V}^t + \boldsymbol{C}_{s'}^t \nabla_s^s \\ \dot{\boldsymbol{\phi}}_m^t = (\boldsymbol{C}_m^s - \boldsymbol{C}_m^{s'})\boldsymbol{\omega}_{tm}^m + \boldsymbol{\varepsilon}_s^s + \boldsymbol{\omega}_{\phi^m} \\ \dot{\boldsymbol{\nabla}}_s^s = 0 \\ \dot{\boldsymbol{\varepsilon}}_s^s = 0 \\ \dot{\boldsymbol{\phi}}_a^t = 0 \end{cases} \tag{38}$$

Model 1 performs with the following advantages compared with Model 2. Firstly, Model 1 is derived based on the G frame not the t frame in Model 2. By using the grid frame as the navigation frame, Model 1 can solve the problem of the meridians convergence. Secondly, the item of harmful acceleration $-(2\delta\boldsymbol{\omega}_{ie}^G + \delta\boldsymbol{\omega}_{eG}^G) \times \boldsymbol{V}_{s'}^G$ is considered in the velocity differential equation of Model 1, which makes it closer to the real dynamic model and so, Model 1 is more accurate than Model 2. Thirdly, the disturbing acceleration caused by the arm-lever effect and ship flexure deformation $\delta \boldsymbol{f}^s$ is omitted form Model 2. The lack of compensating the disturbing acceleration $\delta \boldsymbol{f}^s$ will reduce the TA accuracy [17]. Therefore, Model 1 based TA suits the large azimuth misalignment angle problem in polar areas.

3.2. Observation model

In the case of the large azimuth misalignment angle, velocity and attitude measurements can be used for the observation model to achieve a rapid alignment. The differences of the velocity and attitude between the master and slave SDINS are chosen as the observations, which are defined as:

$$\boldsymbol{Z} = \begin{bmatrix} \delta \boldsymbol{V}^G & \boldsymbol{\phi}_m^G \end{bmatrix}$$

The observation model is expressed in matrix form as:

$$\boldsymbol{Z} = \boldsymbol{H}\boldsymbol{X} + \boldsymbol{v} \tag{39}$$

Where the observation matrix $\boldsymbol{H}$ can be written as:

$$\boldsymbol{H} = \begin{bmatrix} \boldsymbol{I}_{2\times2} & \boldsymbol{0}_{2\times2} & \boldsymbol{0}_{2\times2} & \boldsymbol{0}_{2\times2} & \boldsymbol{0}_{2\times2} \\ \boldsymbol{0}_{3\times3} & \boldsymbol{I}_{3\times3} & \boldsymbol{0}_{3\times3} & \boldsymbol{0}_{3\times3} & -\boldsymbol{C}_{s'}^G \end{bmatrix} \tag{40}$$

The measurement noise vectors $\boldsymbol{v}$ is independent Gaussian white noise $\boldsymbol{v}_i \sim N(0, \boldsymbol{R}_i)$.

Where $\boldsymbol{R}$ is measurement noise covariance matrix.

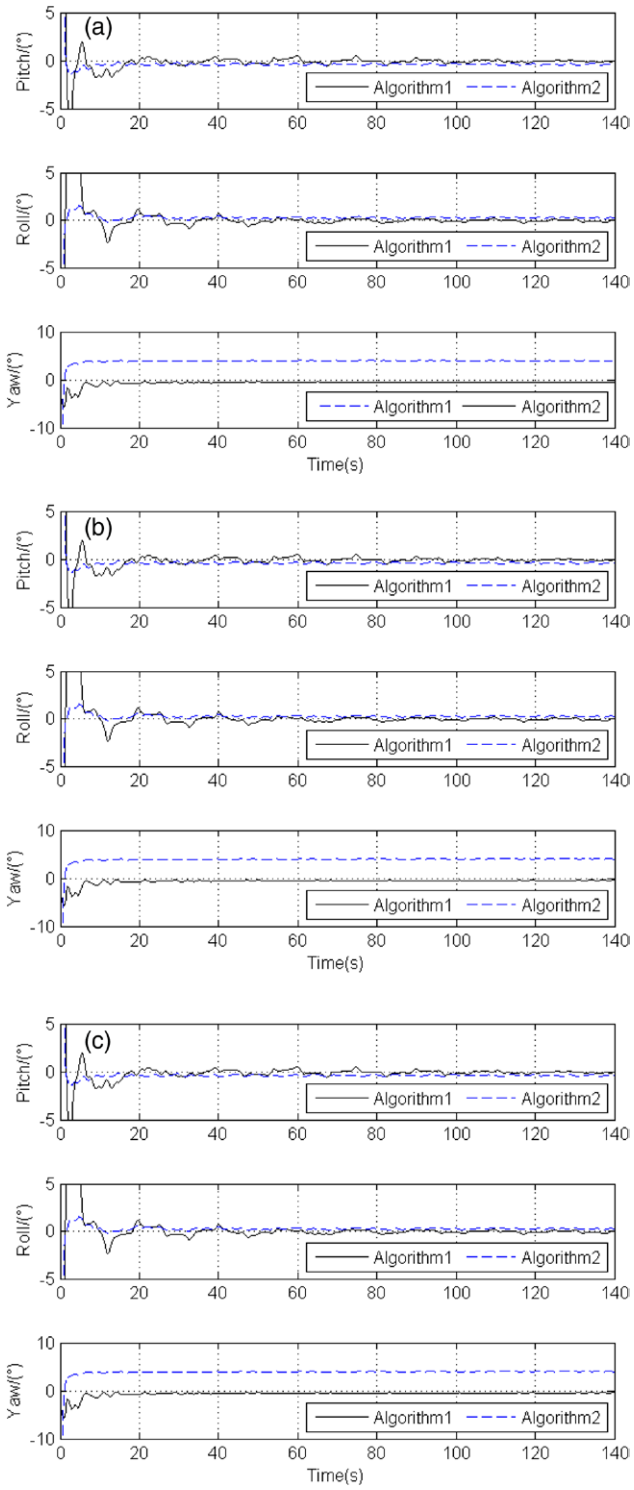

Figure 3. (a) TA results when ship is static. (b) TA results when ship sails in uniform linear motion. (c) TA results when ship sails is in linear motion with constant acceleration.

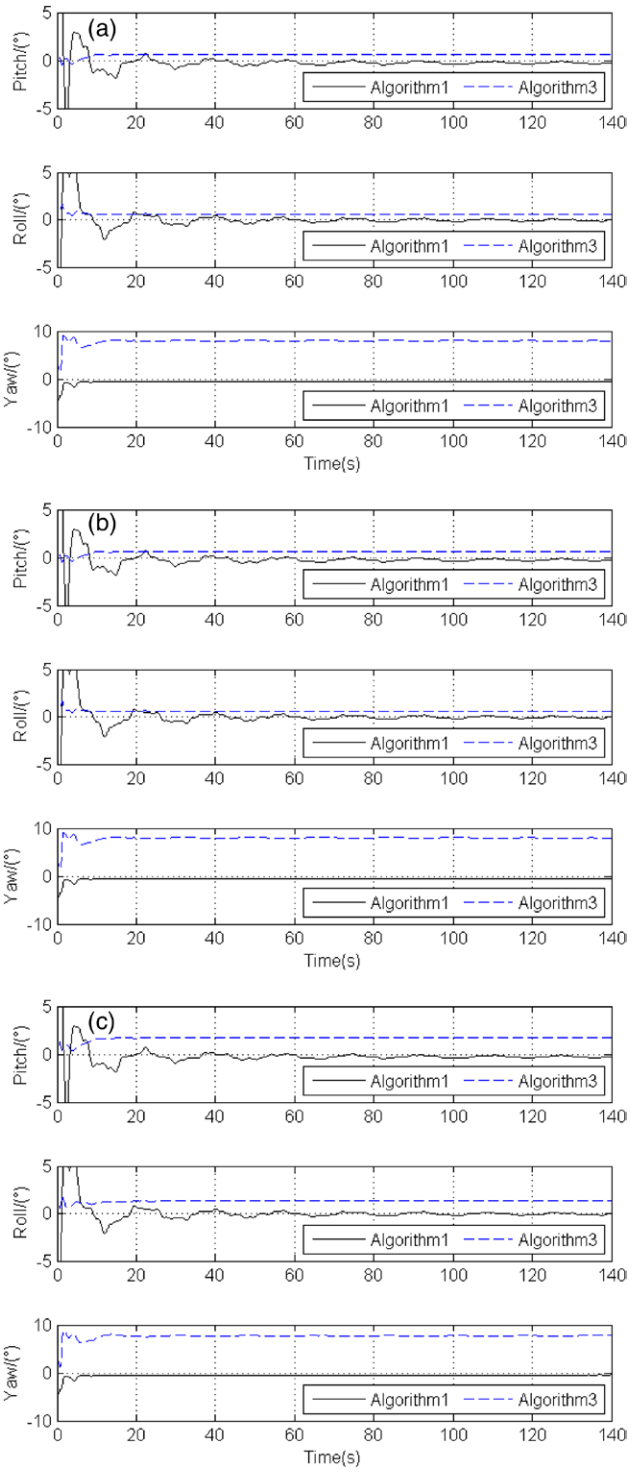

Figure 4. (a) TA results when ship is static. (b) TA results when ship sails in uniform linear motion. (c) TA results when ship sails is in linear motion with constant acceleration.

4. Results and discussions

The polar TA algorithm is designed based on the grid frame. Also, a nonlinear UKF is employed for the TA to solve the problem of large azimuth misalignment angle. Simulations and experiments are conducted to verify the necessity of the grid frame for polar TA and the performance of the UKF.

4.1. Simulation and experiment conditions

When a ship is sailing in practical environments, sea states and maneuvers of the ship are variable. To estimate the performances of the designed TA in practical environments, two sea states and three ship maneuvers are considered. The sea states include calm and medium sea states, and the maneuvers include static, uniform linear motion and linear motion with

Table 3. TA results in the calm sea state.

Parameters	Algorithm	Static	Uniform linear motion	Linear motion with constant acceleration
pitch/(°)	Algorithm 1	−0.2811	−0.2811	−0.2846
	Algorithm 3	0.6314	0.6304	1.755
roll/(°)	Algorithm 1	−0.0295	−0.0303	−0.0266
	Algorithm 3	0.6075	0.6082	1.349
yaw/(°)	Algorithm 1	−0.5225	−0.5225	0.4405
	Algorithm 3	7.995	7.994	7.778

Table 4. TA results in the medium sea state.

Parameters	Algorithm	Static	Uniform linear motion	Linear motion with constant acceleration
pitch/(°)	Algorithm 1	−0.0646	−0.0644	−0.0570
	Algorithm 3	0.6624	0.6913	0.6922
roll/(°)	Algorithm 1	−0.0113	−0.0121	−0.0119
	Algorithm 3	0.5688	0.6219	0.6513
yaw/(°)	Algorithm 1	−0.4809	−0.4809	−0.3972
	Algorithm 3	7.784	7.781	7.728

Table 5. Experimental results of algorithms 1 and 2.

Parameters	Algorithm	Static in clam sea state	Uniform linear motion in medium sea state	Linear motion with constant acceleration in medium sea state
pitch/(°)	Algorithm 1	−0.2186	−0.2184	−0.1401
	Algorithm 2	−0.7809	−0.666	−1.396
roll/(°)	Algorithm 1	0.1074	0.1065	0.0383
	Algorithm 2	0.6519	0.8093	1.197
yaw/(°)	Algorithm 1	−0.5876	−0.5875	−0.7487
	Algorithm 2	5.541	4.992	5.072

constant acceleration. The main involved parameters are set as follows:

(1) In this paper, the attitude of the ship is set as sine functions. In a calm sea state, the amplitude/period of pitch angle, roll angle and yaw angle are 1°/3 s, 1°/5 s and 1°/7 s, respectively. In a medium sea state, the amplitude/period of pitch angle, roll angle and yaw angle are 10°/3 s, 9°/5 s and 7°/7 s, respectively. The initial phase is 0 °and the initial heading is 45 °.

(2) The velocity of ship is set as 10 nmile h^{-1} in the case of uniform linear motion. In linear motion with constant acceleration, the initial velocity and acceleration are set as 10 nmile h^{-1} and 0.1 g, respectively. The initial latitude φ and longitude λ are set as 80.7796° and 126.6705°, respectively.

(3) In the simulation, the gyro constant drift is 0.01°/h and the gyro random drift variance is 0.001°/h. The accelerometer constant drift is $1 \times 10^{-4} g_0$ and the accelerometer random drift variance is $1 \times 10^{-5} g_0$. The initial errors of roll, pitch and yaw angles are set as 0.5 °, 0.5 ° and 10 °, respectively. Simulation time is 140 s. Filtering period is 0.1 s.

(4) The initial state estimation covariance matrix P_0, system noise covariance matrix Q_0, and measurement noise covariance matrix R_0 are set as follows:

$$P_0 = \mathrm{diag}\left\{\begin{array}{l}(0.1\,\mathrm{m\,s^{-1}})^2, (0.1\,\mathrm{m\,s^{-1}})^2, (0.5\,°)^2, (0.5\,°)^2, \\ (10\,°)^2, (1\times10^{-4}g_0)^2, (1\times10^{-4}g_0)^2, (0.01(°)/h)^2, \\ (0.01(°)/h)^2, (0.01(°)/h)^2, (0.5\,°)^2, (0.5\,°)^2, (10\,°)^2\end{array}\right\}$$

$$Q_0 = \mathrm{diag}\left\{\begin{array}{l}(5\times10^{-4}g_0)^2, (5\times10^{-4}g_0)^2, \\ (0.05(°)/h)^2, (0.05(°)/h)^2, (0.05(°)/h)^2\end{array}\right\}$$

$$R_0 = \mathrm{diag}\left\{\begin{array}{l}(0.1\,\mathrm{m\,s^{-1}})^2, (0.1\,\mathrm{m\,s^{-1}})^2, \\ (0.001\,°)^2, (0.001\,°)^2, (0.001\,°)^2\end{array}\right\}$$

4.2. Simulation results and discussions

The TA algorithm proposed in this paper is defined as algorithm 1. Meanwhile, the typical non-polar TA algorithm, which is presented in [14], is defined as algorithm 2. In order to increase the simulation contrast, the linear TA algorithm based on grid frames, which is presented in [12], is defined as algorithm 3. Besides, TA algorithms can be evaluated by the accuracy of the measurement misalignment angles ϕ_m^G estimates.

4.2.1. The selection of navigation frames for polar TA. Both algorithms 1 and 2 adopt nonlinear models and use UKF to solve the TA problems of the large misalignment angle. The difference between them is the selection of navigation

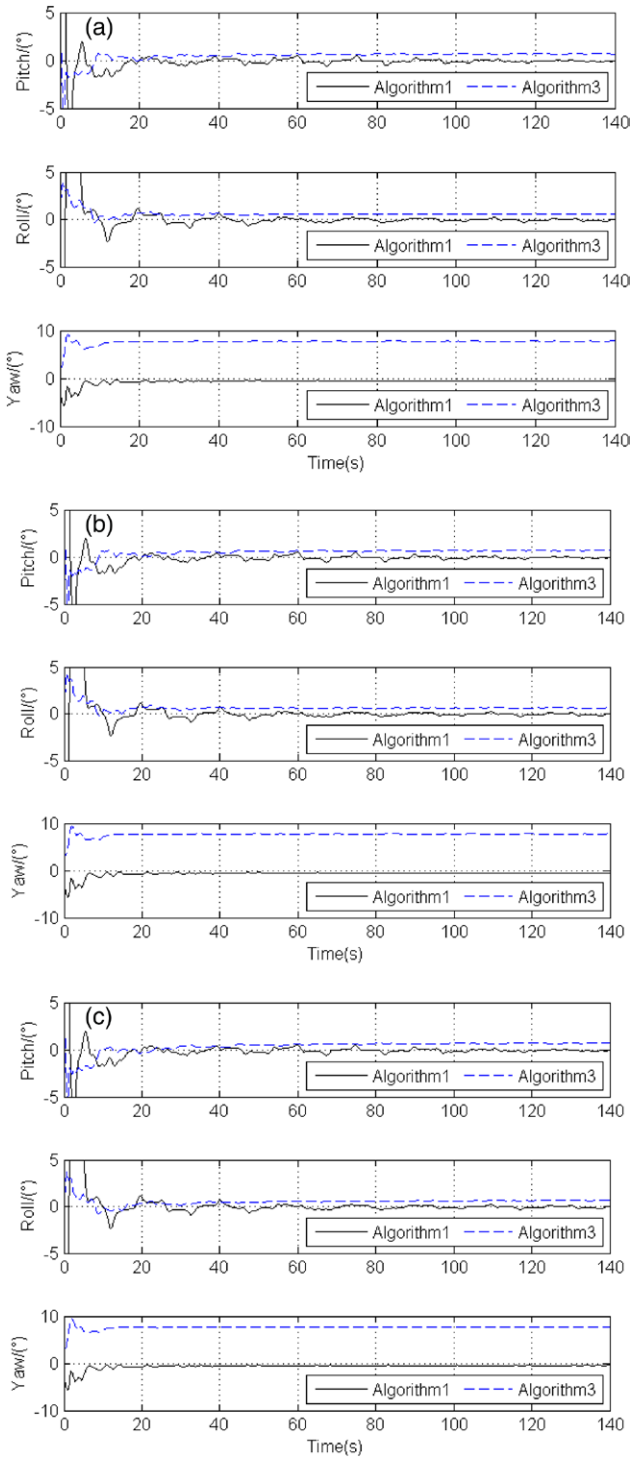

Figure 5. (a) TA results when ship is static. (b) TA results when ship sails in uniform linear motion. (c) TA results when ship sails in linear motion with constant acceleration.

frame. Algorithm 2 selects geographic frames for the non-polar region while this paper selects grid frames for the polar region.

In a calm sea state, TA results under different maneuvers are shown in figure 2 and table 1.

In a medium sea state, TA results under different maneuvers are shown in figure 3 and table 2.

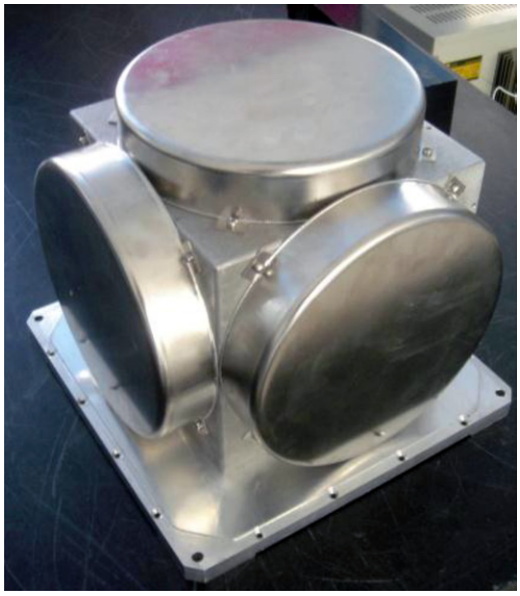

Figure 6. Inertial measurement unit (IMU).

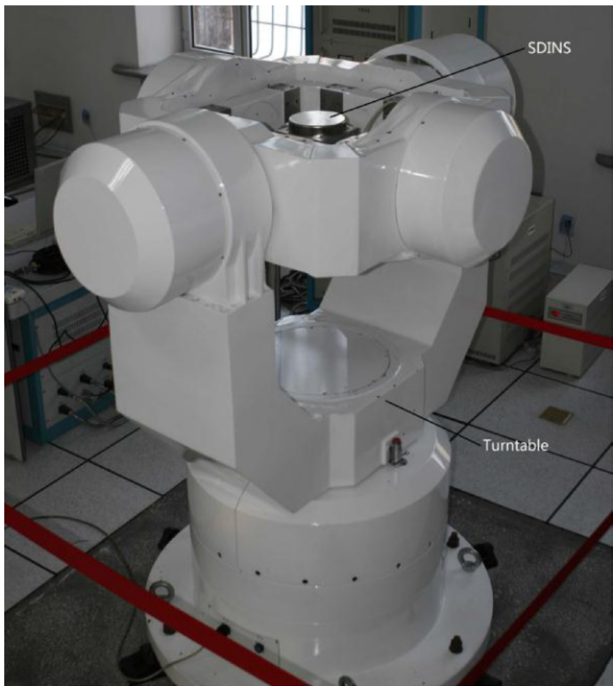

Figure 7. High-precision, three-axis turntable and SDINS.

As shown in figures 2 and 3, compared with algorithm 2, the azimuth accuracy of algorithm 1 is significantly higher. Detailed data of TA results are given as follows:

As shown in table 1, the pitch errors of algorithm 1 reduce to around 60% than the errors of algorithm 2, and the roll errors of algorithm 1 reduce to around 12% than the errors of algorithm 2. As shown in table 2, the pitch errors of algorithm 1 reduce to around 20% than the errors of algorithm 2, and the roll errors of algorithm 1 reduce to around 5% than the errors of algorithm 2. TA performance of algorithm 1 is better than that of algorithm 2 because algorithm 2 is based on geographic frames. Meanwhile, algorithm 1 based on grid frames can avoid the navigation problems caused by meridian

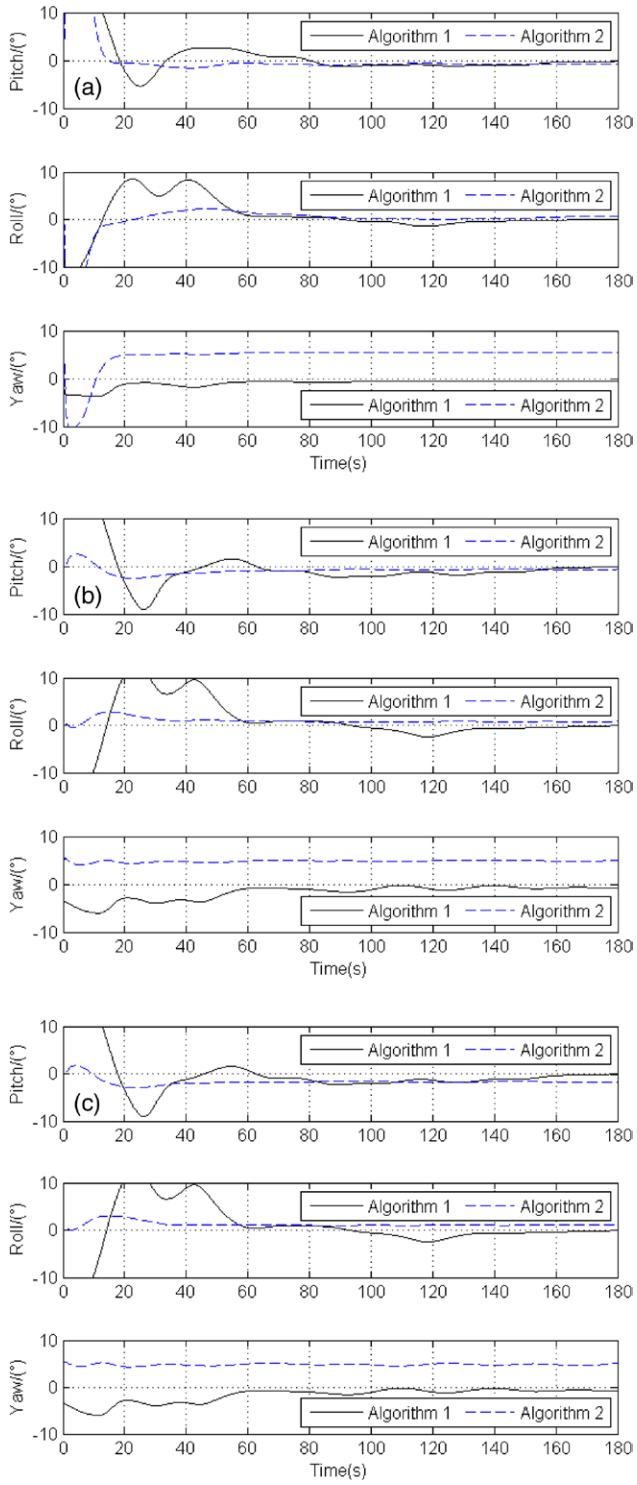

Figure 8. (a) Experimental results of algorithms 1 and 2 in a calm state when ship is static. (b) Experimental results of algorithms 1 and 2 in a medium sea state when ship sails in uniform linear motion. (c) Experimental results of algorithms 1 and 2 in medium sea state when ship sails in linear motion with constant acceleration.

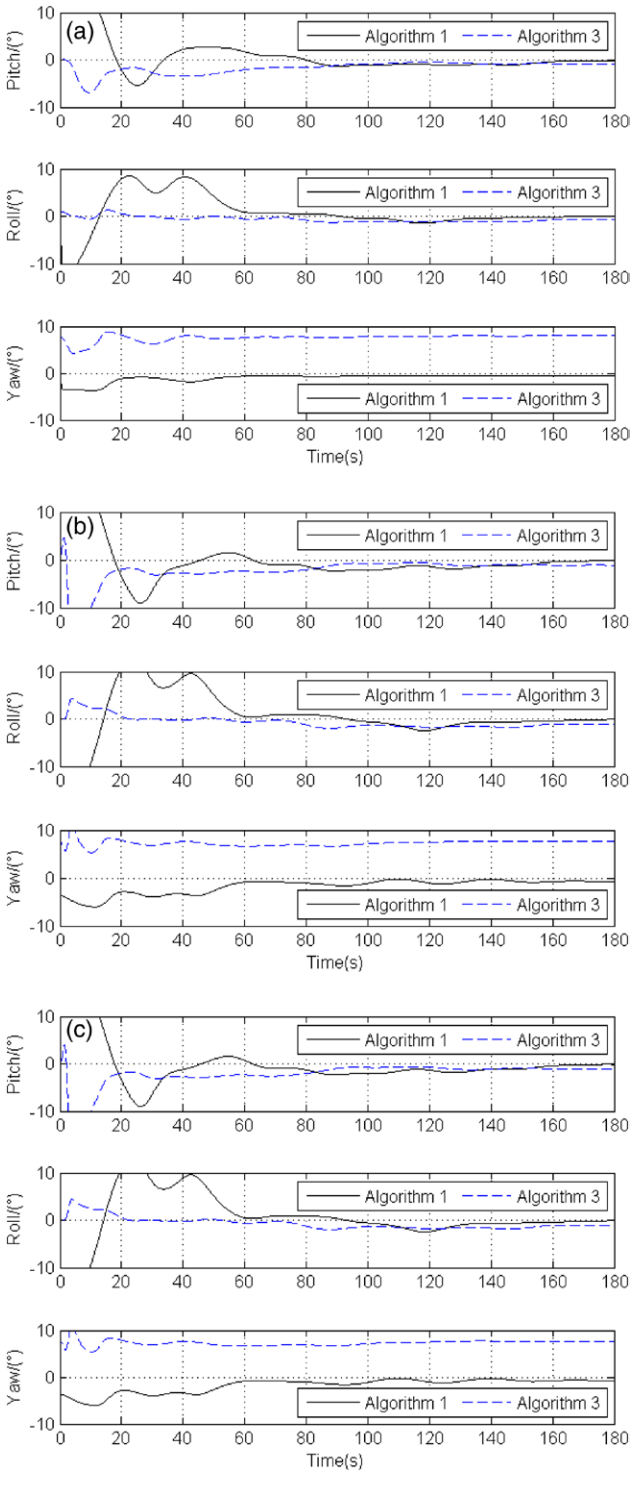

Figure 9. (a) Experimental results of algorithms 1 and 3 in calm state when ship is static (b) Experimental results of algorithms 1 and 3 in medium sea state when ship sails in uniform linear motion. (c) Experimental results of algorithms 1 and 3 in medium sea state when ship sails in linear motion with constant acceleration.

convergence. Therefore, it is necessary to choose grid frames as navigation frames.

4.2.2. The UKF performance in the case of large azimuth misalignment angle. Both algorithm 1 and algorithm 3 choose grid frames as navigation frames. The differences between them are the models and filtering methods. Algorithm 3 processes its linear models by KF, which is unsuitable for the nonlinear model with the large azimuth misalignment angle.

In a calm sea state, TA results under different maneuvers are shown in figure 4 and table 3.

Table 6. Experimental results of algorithms 1 and 3.

Parameters	Algorithm	Static in clam sea state	Uniform linear motion in medium sea state	Linear motion with constant acceleration in medium sea state
pitch/(°)	Algorithm 1	−0.2186	−0.2184	−0.1401
	Algorithm 3	−0.9304	−1.219	−1.214
roll/(°)	Algorithm 1	0.1074	0.1065	0.0383
	Algorithm 3	−0.7029	−1.137	−1.132
yaw/(°)	Algorithm 1	−0.5876	−0.5875	−0.7487
	Algorithm 3	7.977	7.694	7.693

In a medium sea state, TA results under different maneuvers are shown in figure 5 and table 4.

As shown in figures 4 and 5, compared with the linear algorithm 3, employing algorithm 1 in this article, the azimuth accuracy is significantly higher. Detailed data of TA results are given as follows:

As shown in table 3, the pitch errors of algorithm 1 reduce to around 45% than the errors of algorithm 3, and the roll errors of algorithm 1 reduce to around 5% than the errors of algorithm 3. As shown in table 5, the pitch errors of algorithm 1 reduce to around 10% than the errors of algorithm 3, and the roll errors of algorithm 1 reduce to around 2% than the errors of algorithm 3. TA performance of algorithm 1 is better than that of algorithm 3 because the models of algorithm 3 are linear. In the condition of large azimuth misalignment angle, linear KF models cannot estimate state of system effectively. Therefore, the polar TA based on the UKF can be effective to improve not only the TA accuracy but also the system robustness.

4.3. Experimental results and discussions

Because of the geographic restriction, the experiment is conducted in the form of semi-physical simulation.

The angular velocity $\widehat{\boldsymbol{\omega}}_{ib}^{b}$ measured by gyroscope can be expressed as

$$\widehat{\boldsymbol{\omega}}_{ib}^{b} = \boldsymbol{\omega}_{ib}^{b} + \delta\boldsymbol{\omega}_{is}^{s} \tag{41}$$

Where $\boldsymbol{\omega}_{ib}^{b}$ is the true angular velocity without biases.

The gyro drifts $\delta\boldsymbol{\omega}_{is}^{s}$ can be extracted from measured data. The real angular velocity $\boldsymbol{\omega}_{ib}^{b}$ in the polar region can be calculated by simulation. Therefore, the experimental gyroscope outputs in the polar region can be simulated by the gyroscope measurements in nonpolar region. Similarly, the experimental accelerometer outputs can be obtained in this way.

The experimental data is provided by the inertial measurement unit (IMU), which is shown in figure 6. The IMU consists of three-axis gyroscopes and accelerometers. The IMU-based SDINS is installed on a high-precision three-axis turntable as shown in figure 7.

The drifts of gyroscopes and accelerometers can be obtained from the real test, which are shown as follows.

The three-axis gyro constant drifts are $6.0840 \times 10^{-9}\,\mathrm{rad\,s^{-1}}$, $-4.6614 \times 10^{-9}\,\mathrm{rad\,s^{-1}}$, $-1.2844 \times 10^{-8}\,\mathrm{rad\,s^{-1}}$, respectively. The three-axis accelerometer constant drifts are $5.3470 \times 10^{-6}\,\mathrm{m\,s^{-2}}$, $2.1293 \times 10^{-6}\,\mathrm{m\,s^{-2}}$, $-7.7923 \times 10^{-6}\,\mathrm{m\,s^{-2}}$, respectively. The three-axis gyro random drifts variances are $3.469 \times 10^{-6}\,\mathrm{rad\,s^{-1}}$, $3.749 \times 10^{-6}\,\mathrm{rad\,s^{-1}}$, $1.464 \times 10^{-6}\,\mathrm{rad\,s^{-1}}$, respectively. The three-axis accelerometer random drifts variances are $0.00145\ \mathrm{m\,s^{-2}}$, $0.001852\ \mathrm{m\,s^{-2}}$, $0.0003957\ \mathrm{m\,s^{-2}}$, respectively.

Other conditions can be seen in section 4.1.

Three typical maneuvers, namely static in the calm sea state, uniform linear motion in the medium sea state and linear motion with constant acceleration in the medium sea state, are considered in experiments. The experimental results are also expressed by the estimated values of measurement misalignment angles ϕ_{m}^{G}.

Experimental results of algorithms 1 and 2 under the three typical maneuvers are shown in figure 8 and table 5.

Experimental results of algorithms 1 and 3 under the three typical maneuvers are shown in figure 9 and table 6.

Detailed data of experimental results are given as follows

As shown in figure 8 and table 5, experimental results further verify that the TA performance of algorithm 1 is better than that of algorithm 2. This benefits from the selection of grid frames as navigation frames in algorithm 1. Also, experimental results in figure 9 and table 6 show that TA performance of algorithm 1 is better than that of algorithm 3 due to the nonlinear models of algorithm 1.

The experimental results imply that the shipborne SDINS based on algorithm 1 is capable of working effectively in polar regions. Furthermore, the SDINS can perform with good accuracy even in the case of large misalignment angles.

5. Conclusions

The polar TA algorithm with nonlinear model is proposed to solve the problem of a large azimuth misalignment angle in the polar regions. The navigation error equations are firstly derived based on the grid frame. The nonlinear UKF models are designed by combing the error equations and the velocity plus attitude matching method. A UKF is applied to estimate the misalignment parameters. The simulation and experimental results have demonstrated the performance of the proposed TA algorithm.

Acknowledgment

This work was partially funded by the National Nature Science Foundation of China under grant No. 61374007, No. 61273081 and No. 61104036. The authors would like to thank all the editors and anonymous reviewers for improving this article.

References

[1] Li Q, Ben Y Y, Sun F and Huo L 2014 Transversal strapdown INS and damping technology for marine in polar region *Position, Location and Navigation Symp.—Plans (Monterey, CA, 5–8 May 2014)* (IEEE/ION) pp 1365–70

[2] Zhao C L, Wu W Q and Lian J X 2014 Research on rotating modulation inertial navigation system error characteristics simulation method in polar area *IEEE Chinese Guidance, Navigation and Control Conf. (Yantai China, 8–10 August 2014)* pp 2790–4

[3] Yahaya M H and Kamarudin M N 2008 Analysis of GPS visibility and satellite-receiver geometry over different latitudinal region *Int. Symp. on Geoinformation* pp 1–8

[4] Zhang Q, Niu X J, Zhang H P and Shi C 2013 Using Allan variance to evaluate the relative accuracy on different time scales of GNSS/INS systems *Meas. Sci. Technol.* **24** 085006

[5] Esmat B 2007 *Introduction to Modern Navigation Systems* (Singapore: World Scientific)

[6] Zhang C B, Tian W F and Jin Z H 2004 A novel method improving the alignment accuracy of a strapdown inertial navigation system on a stationary base *Meas. Sci. Technol.* **15** 765–9

[7] Silson P M G 2011 Coarse alignment of ship's strapdown inertial attitude reference system using velocity loci *IEEE Trans. Instrum. Meas.* **60** 1930–41

[8] Kain J E and Cloutier J R 1989 Rapid transfer alignment for tactical weapon applications *AIAA Guidance, Navigation and Control Conf.* pp 1290–1300

[9] Greenaway K R and Gates M D 2009 *Polar Air Navigation—a Record* (Canada: Art Bookbindery)

[10] Li Q, Ben Y Y, Yu F and Sun F 2015 System reset of transversal strapdown INS for ship in polar region *Measurement* **60** 247–57

[11] Zhou Q, Qin Y Y, Fu Q W and Yue Y Z 2013 Grid mechanization in inertial navigation systems for transpolar aircraft *J. Northwestern Polytech. Univ.* **31** 210–7 (in Chinese)

[12] Wu F, Qin Y Y and Zhou Q 2013 Airborne weapon transfer alignment algorithm in polar regions *J. Chin. Inertial Technol.* **21** 141–6 (in Chinese)

[13] Chang L, Hu B Q, Li A and Qin F J 2013 Strapdown inertial navigation system alignment based on marginalized unscented Kalman filter *Sci. Meas. Technol. Lett.* **7** 128–38

[14] Wei X T and Gao L 2012 Transfer alignment of carrier-born aircraft under large azimuth misalignment angle *J. Chin. Inertial Technol.* **20** 552–6 (in Chinese)

[15] Reid J, Tucker M and Dayan R 1980 An extended Kalman filter for the estimation of transfer alignment errors to an airborne vehicle *AIAA Guidance Navigation and Control Conf.* pp 54–61

[16] Hao Y L, Xiong Z L, Wang W and Sun F 2006 Rapid transfer alignment based on unscented Kalman filter *Proc. of the 2006 American Control Conf.* pp 2215–20

[17] Ding G Q, Zhou W D, Hao Y L and Sun F 2009 The impact of arm-lever effect error based large initial misalignment transfer alignment technology study *Int. Workshop on Intelligent Systems and Applications* pp 1–6